

Longitudinal Deep Kernel Gaussian Process Regression

Junjie Liang, Yanting Wu, Dongkuan Xu, Vasant Honavar
The Pennsylvania State University
{jul672, yxw514, dux19, vhonavar}@ist.psu.edu

Abstract

Gaussian processes offer an attractive framework for predictive modeling from longitudinal data, *i.e.*, irregularly sampled, sparse observations from a set of individuals over time. However, such methods have two key shortcomings: (i) They rely on ad hoc heuristics or expensive trial and error to choose the effective kernels, and (ii) They fail to handle multilevel correlation structure in the data. We introduce Longitudinal deep kernel Gaussian process regression (L-DKGPR), which to the best of our knowledge, is the only method to overcome these limitations by fully automating the discovery of complex multilevel correlation structure from longitudinal data. Specifically, L-DKGPR eliminates the need for ad hoc heuristics or trial and error using a novel adaptation of deep kernel learning that combines the expressive power of deep neural networks with the flexibility of non-parametric kernel methods. L-DKGPR effectively learns the multilevel correlation with a novel additive kernel that simultaneously accommodates both time-varying and the time-invariant effects. We derive an efficient algorithm to train L-DKGPR using latent space inducing points and variational inference. Results of extensive experiments on several benchmark data sets demonstrate that L-DKGPR significantly outperforms the state-of-the-art longitudinal data analysis (LDA) methods.

1 Introduction

Longitudinal studies, which involve repeated observations, taken at irregularly spaced time points, for a set of individuals over time, are ubiquitous in many applications, *e.g.*, in health, cognitive, social, and economic sciences. Such studies are used to identify the time-varying as well as the time-invariant factors associated with a particular outcome of interest, *e.g.*, health risk [1]. Longitudinal data typically exhibit longitudinal correlation (LC), *i.e.*, correlations among the repeated observations of a given individual over time; and cluster correlation (CC), *i.e.*, correlations among observations across individuals, *e.g.*, due to the characteristics that they share among themselves *e.g.*, age, demographics factors; or both, *i.e.*, multilevel correlation (MC). In general, the structure of MC can be complex and a priori unknown. Failure to adequately account for the structure of MC in predictive modeling from longitudinal data can lead to misleading statistical inferences [2, 3]. It can be non-trivial to choose a suitable correlation structure that reflects the correlations present in the data. The relationships between the covariates and outcomes of interest can be highly complex and non-linear. Furthermore, modern applications often call for LDA methods that scale gracefully with increasing number of variables, the number of individuals, and the number of longitudinal observations per individual.

LDA methods have been extensively studied for decades [1, 4]. Conventional LDA methods fall into two broad categories: (i) marginal models and (ii) conditional models. Marginal models rely on assumptions about the marginal association among the observed outcomes. The generalized estimating equations (GEE) [5], where a working correlation matrix is specified to model the marginal association among the observed outcomes, offer an example of marginal models. The parameters of marginal

models are often shared by all individuals in the population, yielding *population-averaged* effects or *fixed* effects. Conditional models on the other hand avoid directly specifying the full correlation matrix by distinguishing *random* effects, *i.e.*, parameters that differ across individuals, from fixed effects, so as to estimate the individual parameters conditioned on the population parameters. A popular example of conditional models is the generalized linear mixed-effects models (GLMM) [6]. Despite much work on both marginal and conditional models [7, 8, 9, 3], many of the challenges, especially the choice of correlation structure, and the selection of variables to model random versus fixed effects, and the scalability of the methods remain to be addressed.

More recently, there is a growing interest in Gaussian processes (GP) [10, 11] for LDA because of their advantages over conventional parametric LDA methods: (i) GP make fewer assumptions about the underlying data distribution by dispensing with the need to choose a particular parametric form of the nonlinear predictive model; (ii) GP permit the use of parameterized kernels to model the correlation between observed outcomes, to cope with data sampled at irregularly spaced time points, by interpolating between samples; (iii) The interpretability of GP models can be enhanced by choosing modular kernels that are composed of simpler kernels that capture the shared correlation structure of a subset of covariates, and (iv) GP models can flexibly account for both longitudinal and cluster correlations in the data. For example, Cheng *et al.* [11] utilize an additive kernel for Gaussian data and employ a step-wise search strategy to select the kernel components and covariates that optimize the predictive accuracy of the model. Timonen *et al.* [12] consider a heterogeneous kernel to model individual-specific (random) effects in the case of non-Gaussian data. Despite their advantages, existing GP based approaches to LDA suffer from several shortcomings that limit their applicability in real-world settings: (i) The choice of an appropriate kernel often involves a tedious, often expensive and unreliable, process of trial and error [13] or ad hoc heuristics for identifying a kernel or selecting a subset of kernels from a pool of candidates [11]. (ii) Suboptimal choice of kernels can fail to adequately model the complex MC structure in the data. (iii) They do not scale to thousands of covariates and/or millions of data points that are common in modern LDA applications.

Overview of contributions. We introduce Longitudinal deep kernel Gaussian process regression (L-DKGPR), which to the best of our knowledge, is the only method to fully automate the discovery of complex multi level correlation structure from longitudinal data. L-DKGPR inherits the attractive features of GP while overcoming their key limitations. Specifically, L-DKGPR eliminates the need for ad hoc heuristics or trial and error by using a deep kernel learning method [14] that combines the expressive power of deep neural networks with the flexibility of non-parametric kernel methods. L-DKGPR effectively models multilevel correlation structure induced by the time-invariant individual-specific random effects and the time-varying fixed effects using a novel additive kernel. We introduce an EM-like algorithm that combines latent space inducing points and stochastic variational inference for effective training of L-DKGPR. We report results of extensive experiments using both simulated and real-world benchmark longitudinal data that show that L-DKGPR significantly outperforms, by large margins, the popular GLMM, GEE baselines as well as several state-of-the-art non-linear LDA methods [3, 12].

2 Preliminaries

Notations. We denote a longitudinal data set by $\mathcal{D} = (X, \mathbf{y})$, where $X \in \mathbb{R}^{N \times P}$ is the covariate matrix and $\mathbf{y} \in \mathbb{R}^{N \times 1}$ is the vector of measured outcomes. We denote a row in X by x_{it} , with i, t indexing the individual and the time for the observation respectively. Because the observations for each individual are irregularly sampled over time, we have for each individual i , a submatrix $X_i \in \mathbb{R}^{N_i \times P} \subset X$, where N_i is the number of observations available for the individual i . If we denote by I be the number of individuals in \mathcal{D} , the covariate matrix X is given by $X^\top = (X_1^\top, \dots, X_I^\top)^\top$. Accordingly, the outcomes \mathbf{y} are given by $\mathbf{y}^\top = (\mathbf{y}_1^\top, \dots, \mathbf{y}_I^\top)^\top$.

Gaussian Process. A Gaussian process (GP) is a stochastic process, *i.e.*, a distribution over functions or an infinite collection of (real-valued) random variables, such that any finite subset of random variables has a multivariate Gaussian distribution [15]. A kernel describes the covariance of the random variables that make up the GP. More precisely, if a function $f : \mathcal{X} \rightarrow \mathbb{R}$ has a GP prior $f \sim \mathcal{GP}(\mu, k_\gamma)$ where μ is the mean function and $k_\gamma(\cdot, \cdot)$ is a (positive semi-definite) kernel function parameterized by γ , then any finite collection of components of f (denoted as \mathbf{f}) has a multivariate Gaussian distribution $(\mathbf{f}|X) \sim \mathcal{N}(\mu(X), K_{XX})$, where $\mu(X)$ is the mean vector, and

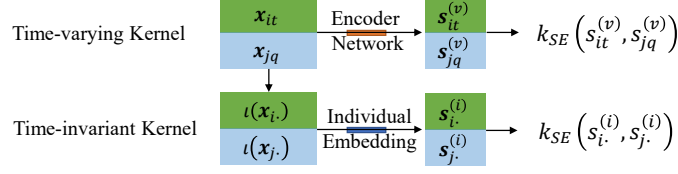


Figure 1: Structure of the deep kernels.

$(K_{XX})_{ij} = k_\gamma(\mathbf{x}_i, \mathbf{x}_j)$ is the covariance matrix. In the regression setting, the function f is treated as an unobserved signal linked to the outcomes through a (typically Gaussian) likelihood function, such that $(y|\mathbf{f}) \sim \mathcal{N}(\mathbf{f}, \sigma^2 \mathbf{I})$.

Additive GP is a special case of GP where unobserved signal is expressed as the sum of J independent signal components, *i.e.*, $f = \sum_{j=1}^J \alpha_j f^{(j)}$, where $\alpha = \{\alpha_j\}_{j=1}^J$ are the coefficients associated with the individual components. In practice, each signal component is computed on a (typically small [11, 12]) subset of the observed covariates in \mathbf{x} . The fact that each signal component has a GP prior ensures that the joint signal f is also GP. Additive GP allows using different kernel functions for different signal components, so to model the shared correlation structure of a subset of covariates, thus enhancing the interpretability of the resulting GP. More importantly, it permits the time-varying and time-invariant effects to be modeled using different kernel functions, which is especially attractive in modeling longitudinal data.

3 Longitudinal Deep Kernel Gaussian Process Regression

Predictive modeling from longitudinal data typically requires solving two sub-problems: (i) Extracting the time-varying and time-invariant information from the observed data to estimate the underlying multilevel correlation structure; and (ii) using the estimated correlation structure to predict the future outcomes. In what follows, we describe our solutions to both sub-problems.

3.1 Modeling the Multilevel Correlation using Deep Kernels

Recall that longitudinal data exhibit complex correlations arising from the interaction between time-varying effects and time-invariant effects. Hence, we decompose the signal function f into two parts, *i.e.*, $f^{(v)}$ which models the time-varying effects and $f^{(i)}$, which models the time-invariant effects. The result is a probabilistic model that can be specified as follows:

$$(y|\mathbf{f}) \sim \mathcal{N}(\mathbf{f}, \sigma^2 \mathbf{I}), \quad f = \alpha^{(v)} f^{(v)} + \alpha^{(i)} f^{(i)} \quad (1)$$

$$(\mathbf{f}^{(v)}|X) \sim \mathcal{N}(\boldsymbol{\mu}^{(v)}(X), k_\gamma^{(v)}(X, X)), \quad (\mathbf{f}^{(i)}|X) \sim \mathcal{N}(\boldsymbol{\mu}^{(i)}(X), k_\phi^{(i)}(X, X)) \quad (2)$$

We denote the kernel parameters for time-varying effects and time-invariant effects respectively by γ and ϕ . The mean functions $\boldsymbol{\mu}^{(v)}, \boldsymbol{\mu}^{(i)}$, if unknown, can be estimated from data. In this study, without loss of generality, following [15, 14, 16, 11, 12], we set $\boldsymbol{\mu}^{(v)} = \boldsymbol{\mu}^{(i)} = 0$. Assuming that $\mathbf{f}^{(v)}$ and $\mathbf{f}^{(i)}$ are conditionally independent given X , we can express the joint signal distribution \mathbf{f} as follows:

$$(\mathbf{f}|X) \sim \mathcal{N}\left(\mathbf{0}, k_\theta(X, X) = \alpha^{(v)2} k_\gamma^{(v)}(X, X) + \alpha^{(i)2} k_\phi^{(i)}(X, X)\right) \quad (3)$$

Time-varying Kernel $k_\gamma^{(v)}$. We introduce a time-varying kernel to capture the longitudinal correlation in the data. The structure of our time-varying kernel $k_\gamma^{(v)}$ is shown in the upper part of Figure 1. Let $e_\gamma: \mathcal{X} \rightarrow \mathcal{S}^{(v)} \in \mathbb{R}^{D_v}$ be a non-linear encoder function given by a deep architecture parameterized by γ . Given a pair of data points $\mathbf{x}_{it}, \mathbf{x}_{jq}$, where i, j index the individuals and t, q index the observations, the time-varying kernel is given by:

$$k_\gamma^{(v)}(\mathbf{x}_{it}, \mathbf{x}_{jq}) = k_{SE}(e_\gamma(\mathbf{x}_{it}), e_\gamma(\mathbf{x}_{jq})) \quad (4)$$

with k_{SE} denoting the squared exponential kernel [15]. Note that SE kernel is based on Euclidean distance, which is not a useful measure of distance in the high dimensional input space [17]. Hence,

we use a deep neural network [18], specifically, a nonlinear encoder to map the input space to a low-dimensional latent space and then apply the SE kernel to the latent space.

Time-invariant Kernel $k_\phi^{(i)}$. We introduce a time-invariant kernel to capture cluster correlation, *i.e.*, time-invariant correlations among individuals that share similar characteristics. The structure of time-invariant kernel is shown in the bottom part of Figure 1. Let $\iota(\mathbf{x}_{i\cdot}) = i$ be function that identifies the individuals, and $g_\phi : \iota(\mathcal{X}) \rightarrow \mathcal{S}^{(i)} \in \mathbb{R}^{D_i}$ be an embedding function that maps each individual to a vector in the latent space. Then for any pair of data points $\mathbf{x}_{i\cdot}, \mathbf{x}_{j\cdot}$ with arbitrary observation indices, the time-invariant kernel is given by:

$$k_\phi^{(i)}(\mathbf{x}_{i\cdot}, \mathbf{x}_{j\cdot}) = k_{SE}(g_\phi \circ \iota(\mathbf{x}_{i\cdot}), g_\phi \circ \iota(\mathbf{x}_{j\cdot})) \quad (5)$$

3.2 Learning a L-DKGPR model from data

We now proceed to describe how to learn L-DKGPR efficiently and how to make prediction on future data. Because of space constraints, the details of the derivations are relegated to Appendix A.

Model Inference. We leverage a body of existing results to ensure the scalability of our algorithm for learning L-DKGPR. Our approach is inspired by [16], which combines the *inducing points* with variational inference. The idea of inducing points is to reduce the effective number of input data points in X from N to M ($M \ll N$), where M is the number of inducing points, thus greatly simplifying the computation of the GP posterior. Let $Z = \{\mathbf{z}_m\}_{m=1}^M$ be the collection of inducing points, and \mathbf{u} their corresponding signal. Unlike [16], instead of identifying the inducing points in the input space, we specify inducing points from a low-dimensional latent space, which is continuous and easy to optimize, such that $\mathbf{z}_m \in \mathcal{S}$. We define $\iota(\mathbf{z}_m) = I + m$ to distinguish the inducing points from the input data. The signal distribution conditioned on the inducing points is given by:

$$(\mathbf{f}|\mathbf{u}, X, Z) \sim \mathcal{N}(K_{XZ}K_{ZZ}^{-1}\mathbf{u}, \tilde{K}), \quad \tilde{K} = K_{XX} - K_{XZ}K_{ZZ}^{-1}K_{XZ}^\top \quad (6)$$

Let $\Theta = \{\alpha^{(v)}, \alpha^{(i)}, \gamma, \phi, \sigma^2, Z\}$ be the model parameters. We aim to learn the parameters by maximizing the log of marginal likelihood $p(\mathbf{y}|X, Z)$. By assuming a variational posterior over the joint signals $q(\mathbf{f}, \mathbf{u}|X, Z) = q(\mathbf{u}|X, Z)p(\mathbf{f}|\mathbf{u}, X, Z)$, we have (*e.g.*, [16]):

$$\log p(\mathbf{y}|X, Z) \geq \mathbb{E}_{q(\mathbf{f}, \mathbf{u}|X, Z)}[\log p(\mathbf{y}|\mathbf{f})] - \text{KL}[q(\mathbf{u}|X, Z)||p(\mathbf{u}|Z)] \triangleq \mathcal{L} \quad (7)$$

Eq (7) provides the variational evidence lower bound (ELBO). We define the proposal posterior $q(\mathbf{u}|X, Z) = \mathcal{N}(\boldsymbol{\mu}_q, L_q L_q^\top)$. To speed up the computation, we follow the deterministic training conditional (DTC) [19], where \tilde{K} is set to 0 during the training phase, resulting in a deterministic \mathbf{f} w.r.t. \mathbf{u} . Let $A = K_{XZ}K_{ZZ}^{-1}$, by reparameterizing $\mathbf{u} = \boldsymbol{\mu}_q + L_q \boldsymbol{\epsilon}$ with $\boldsymbol{\epsilon} \sim \mathcal{N}(\mathbf{0}, \mathbf{I})$, we can rewrite the ELBO in closed form:

$$\begin{aligned} 2\mathcal{L} = & -2N \log \sigma - \sigma^{-2} (\mathbf{y}^\top \mathbf{y} - 2\mathbf{y}^\top A \boldsymbol{\mu}_q + (A \boldsymbol{\mu}_q)^\top A \boldsymbol{\mu}_q + (A L_q \mathbf{1})^\top A L_q \mathbf{1}) \\ & - \log |K_{ZZ}| + 2 \log |L_q| + M - \text{tr}(K_{ZZ}^{-1} L_q L_q^\top) - \boldsymbol{\mu}_q^\top K_{ZZ}^{-1} \boldsymbol{\mu}_q \end{aligned} \quad (8)$$

where $\mathbf{1}$ is a column vector of ones. We can then compute the partial derivatives of \mathcal{L} w.r.t. the parameters of the proposal posterior $q(\mathbf{u}|X, Z)$ (*i.e.*, $\{\boldsymbol{\mu}_q, L_q\}$) and derive its optimal form, yielding:

$$\boldsymbol{\mu}_q = \sigma^{-2} K_{ZZ} B K_{XZ}^\top \mathbf{y}, \quad L_q (\mathbf{I} + \mathbf{1} \mathbf{1}^\top) L_q^\top = K_{ZZ} B K_{ZZ} \quad (9)$$

with $B^{-1} = K_{ZZ} + \sigma^{-2} K_{XZ}^\top K_{XZ}$. To solve L_q from (9), we first compute the Cholesky decomposition of $\mathbf{I} + \mathbf{1} \mathbf{1}^\top = C C^\top$ and $K_{ZZ} B K_{ZZ} = U U^\top$. We then simplify both side of (9) to $L_q C = U$. L_q can then be solved by exploiting the triangular structure on both sides. We separate the model parameters into two groups, *i.e.*, parameters w.r.t. the proposal posterior $\{\boldsymbol{\mu}_q, L_q\}$ and the remaining parameters Θ , and use an EM-like algorithm to update both groups alternatively. Additional details of the L-DKGPR algorithm are provided in Appendix B.

Prediction. Given the covariate matrix X_* for the test data, the predictive distribution is given by:

$$p(\mathbf{f}_*|X_*, X, y, Z) \simeq \mathcal{N}(K_{X_*Z}(K_{ZZ} + \sigma^2 \mathbf{I})^{-1} \boldsymbol{\mu}_q, K_{X_*X_*} - K_{X_*Z}(K_{ZZ} + \sigma^2 \mathbf{I})^{-1} K_{X_*Z}^\top) \quad (10)$$

Complexity. The time complexity and space complexity of both inference and prediction are $\mathcal{O}(NM^2)$ and $\mathcal{O}(NM)$ respectively, where N is the number of measured outcomes, and M the number of inducing points.

4 Experiments

We compare L-DKGPR to several state-of-the-art LDA methods on simulated as well as real-world benchmark data. The experiments are designed to answer research questions about accuracy, scalability, and interpretability of L-DKGPR: (RQ1) How does the performance of L-DKGPR compare with the state-of-the-art methods on standard longitudinal regression tasks? (RQ2) How does the scalability of L-DKGPR compare with that of the state-of-the-art longitudinal regression models? (RQ3) Can L-DKGPR reliably recover the rich correlation structure from the data? (RQ4) How do the different components of L-DKGPR contribute to its overall performance?

4.1 Data

We used one simulated data set and three real-world longitudinal data sets in our experiments:¹

Simulated data. We construct simulated longitudinal data that exhibit *i.e.*, longitudinal correlation (LC) and multilevel correlation (MC) as follows: The outcome is generated using $y = f(X) + \epsilon$ where $f(X)$ is a non-linear transformation based on the observed covariate matrix X and the residual $\epsilon \sim N(0, \Sigma)$. To simulate longitudinal correlation, we simply set Σ to a block diagonal matrix with non-zero entries for within-individual observations. To simulate multilevel correlation, we first split the individuals into C clusters and assign non-zero entries for the data points in the same cluster. Following [11, 12], we simulate 40 individuals, 20 observations, and 30 covariates for each individual. We vary the number of clusters C from [2, 5].

Study of Women’s Health Across the Nation (SWAN) [20]. SWAN is a multi-site longitudinal study designed to examine the health of women during the midlife years. We consider the task of predicting the CESD score, which is used for screening for depression. Similar to [3], we define the adjusted CESD score by $y = \text{CESD} - 15$, thus $y \geq 0$ indicates depression. The variables of interest include aspects of physical and mental health, and demographic factors such as race and income. The resulting data set has 3,300 individuals, 137 variables and 28,405 records.

General Social Survey (GSS) [21]. The GSS data were gathered over 30 years on contemporary American society collected with the goal of understanding and explaining trends and constants in attitudes, behaviors, and attributes. In our experiment, we consider the task of predicting the self-reported general happiness of 4,510 individuals using 1,553 features and 59,599 records. We follow the same setting in [3], where $y = 1$ indicates happy and $y = -1$ indicates the opposite.

The Alzheimer’s Disease Prediction Of Longitudinal Evolution (TADPOLE) [22]. The TADPOLE challenge involves predicting the symptoms related to Alzheimer’s Disease (AD) within 1-5 years of a group of high-risk subjects. In our experiment, we focus on predicting the ADAS-Cog13 score using the demographic features and MRI measures (Hippocampus, Fusiform, WholeBrain, Entorhinal, and MidTemp). The resulting data set has 1,681 individuals, 24 variables and 8,771 records.

4.2 Experimental Setup

To answer RQ1, we use both simulated data and real-world data. To evaluate the regression performance, we compute the mean and standard deviation of R^2 between the actual and predicted outcomes of each method on each data set across 10 independent runs. We use 50%, 20%, 30% of data for training, validation, and testing respectively.

To answer RQ2, we take data from a subset consisting of 50 individuals with the largest number of observations from each real-world data. We record the run time per iteration of each method on both the 50-individual subset and full data set. Because not all baseline methods implement GPU acceleration, we compare the run times of all the methods without GPU acceleration. We report execution failure if a method fails to converge within 48 hours or generates an execution error [3].

To answer RQ3, we rely mainly on the simulated data since the actual correlation structures underlying the real-world data sets are not known. We evaluate the performance of each method by visualizing the learned correlation matrix. Additionally, we provide a case study of real-world data by comparing and interpreting the correlation matrix recovered by the different methods.

¹Complete of simulated data generation and of real-world data pre-processing are provided in Appendix D.

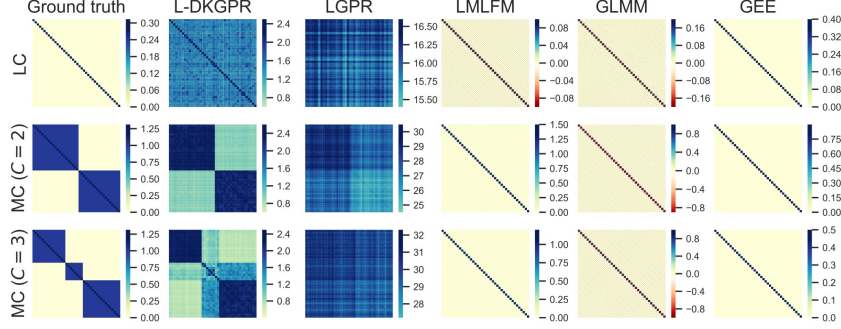


Figure 2: Outcome correlation estimated by all methods on simulated data.

To answer RQ4, we compare the performance of L-DKGPR with L-RBF-GPR, a variant that replaces the learned deep kernel with a simple RBF kernel; and L-DKGPR-, a variant of L-DKGPR without the time-invariant effects. We do not compare L-DKGPR with a variant without the time-varying effects since it gives the same predictions for the same individual regardless of time, which is considered unrealistic in LDA applications.

We compare L-DKGPR with the following baseline methods:

GLMM [23], a conventional multilevel mixed-effect model for longitudinal data. GLMM accounts for data correlations by specifying variables associated with random effects and fixed effects. Because in the general setting, we do not know the exact set of variables that are subject to fixed effects as opposed to random effects, we assume that all variables are subject to random effects conditioned on the individual.

GEE [24], a conventional longitudinal model that is based on generalized estimation equation. GEE accommodates data correlations by factorizing the covariance matrix into a product of a diagonal variance matrix and a working parameterized correlation matrix. In our experiment, we use the first-order auto-regressive $AR(1)$ correlation as it delivers the best performance among all choices.

LMLFM [3], a state-of-the-art multilevel mixed-effect model based on factorization machines. In contrast to GLMM that requires expert input to specify the variables associated with random effects and fixed effects, LMLFM automatically distinguishes random effects from fixed effects and selects a subset of predictive variables by optimizing a suitably specified objective function.

LGPR [12], a state-of-the-art Bayesian longitudinal model based on additive GP. LGPR first fits each GP component using a chosen kernel. The final signal function is achieved by a weighted sum of all GP components. In our experiments, a zero-sum kernel is used for categorical covariates and the heterogeneous kernel is used for continuous covariates. Unlike other baselines, LGPR is solved using MCMC, which generally requires a large number of iterations to reach the stationary distribution. In our experiments, the number of MCMC sampling iterations of LGPR is set to 2000.

Implementation. Please refer to Appendix C for detail. We fixed the latent dimension $D_v = D_i = 10$ and number of inducing points $M = 10$ in all experiments. Our codes are available through <https://anonymous.4open.science/r/cce1f2c6-29ff-4941-993d-d597a71ecc8c/>.

4.3 Results

We report the results of our experiments designed to answer the research questions RQ1-RQ4.

RQ1: L-DKGPR vs. baseline methods on standard longitudinal regression tasks

The results are reported in Table 1 and Table 2 for simulated and real-world data sets respectively. In the case of simulated data, we find that both GEE and GLMM fail in the presence of MC with the mean R^2 being negative. This can be explained by the fact that GEE is designed only to handle pure LC, thus fails to account for CC or MC. While GLMM is capable of handling MC, it requires practitioners to specify the cluster structure responsible for CC prior to model fitting. However, in our experiments, the cluster structure is unknown a priori. Hence it is not surprising that GLMM performs poorly. Moreover, we find that although LMLFM outperforms GLMM and GEE in the presence

Table 1: Regression accuracy R^2 (%) comparison on simulated data with different correlation structures

Method	LC	MC ($C = 2$)	MC ($C = 3$)	MC ($C = 4$)	MC ($C = 5$)
L-DKGPR	86.0±0.2	91.3±0.2	99.6±0.2	99.8±0.2	99.8±0.2
LGPR	-37.1±19.1	-123.6±162.0	-26.3±43.2	-9.1±14.8	-0.1±5.9
LMLFM	54.7±15.1	-138.3±121.9	-48.3±123.6	22.6±49.0	36.2±41.1
GLMM	5.3±27.9	-656.3±719.8	-801.4±507.4	-684.1±491.3	-528.7±313.5
GEE	59.0±24.5	-636.1±606.0	-703.6±465.8	-665.6±554.3	-516.5±457.5

Table 2: Regression accuracy R^2 (%) on real-world data sets. We use ‘N/A’ to denote execution error.

Data sets	N	I	P	L-DKGPR	LGPR	LMLFM	GLMM	GEE
TADPOLE	595	50	24	44.0±5.6	-261.1±9.0	8.7±5.1	50.8±5.5	-11.4±4.8
SWAN	550	50	137	46.8±4.9	-16.6±12.7	38.6±4.2	40.1±7.7	46.4±8.0
GSS	1,500	50	1,553	19.1±3.7	N/A	15.3±1.4	N/A	-4.6±3.5
TADPOLE	8,771	1,681	24	64.9±1.4	N/A	10.4±0.6	61.9±1.9	17.6±0.7
SWAN	28,405	3,300	137	52.5±0.4	N/A	48.6±2.0	N/A	N/A
GSS	59,599	4,510	1,553	56.9±0.1	N/A	54.8±2.2	N/A	N/A

of MC, its R^2 is still quite low. This is because LMLFM accounts for only a special case of MC, namely, for CC among individuals observed at the same time points, and not all of the CC present in the data. We find that LGPR performs rather poorly on both simulated and real-world data. This might be due to the fact that LGPR obtains the contributions of each variable to the kernel independently before calculating their weighted sum. Though it is possible to incorporate higher-order interactions between variables into LGPR, doing so requires estimating large numbers of interaction parameters, with its attendant challenges, especially when working with small populations.

In contrast to the baseline methods, L-DKGPR consistently and significantly outperforms the baselines by a large margin. On the real-world data sets, L-DKGPR outperforms the longitudinal baselines in most of the cases. We see that all methods benefit from larger training data sets, *if they can process the data*. The superior performance of L-DKGPR can perhaps be explained by two factors. First, because L-DKGPR uses a learned deep kernel, it is capable of accommodating complex, a priori unknown, possibly nonlinear relationships between the covariates and the outcomes as needed. Second, L-DKGPR does not rely on restrictive, possibly incorrect, assumptions regarding the correlation structure present in the data; Instead, it learns the correlation structure from the data.

RQ2: Scalability of L-DKGPR vs. baseline methods

We see from Table 2 that LGPR, GLMM, and GEE fail to process real-world data sets with large numbers of covariates. Indeed, their computational complexity increases in proportion to P^3 where P is the number of covariates. In contrast, L-DKGPR and LMLFM scale gracefully with an increase in the number of individuals and the number of covariates.²

RQ3: Recovery of correlation structure

The outcome correlations estimated by all methods on the simulated data are shown in Figure 2. It is easy to see that LMLFM, GLMM, and GEE are incapable of recovering MC. We see that LGPR fails to accurately recover the correlation structure present in the data. In the presence of MC with $C > 2$, we see that only one known cluster is correctly recovered. We conjecture that the inferior performance of LGPR is due to the limited expressive power of the kernel functions used by it. In contrast, L-DKGPR is able to recover most of the correlation structure present in the data.

Evaluation of correlation on real-world data is presented in Appendix E.2. To summarize, the resulting multilevel correlation structure revealed by L-DKGPR offers unique and useful insights that contribute to a deeper understanding of individuals from longitudinal observations.

RQ4: Ablation study

² The results for CPU runtimes are reported in Appendix E.1

Table 3: Effect on the regression accuracy R^2 (%) of different components of L-DKGPR

Data sets	P	L-DKGPR	L-DKGPR-	L-RBF-GPR
TADPOLE	24	64.9±1.4	13.2±1.1	55.5±2.4
SWAN	137	52.5±0.4	29.0±3.2	5.4±1.6
GSS	1,553	56.9±0.1	56.2±0.1	-14±0.4

Regression accuracy comparison on complete real-world data sets is shown in Table 3.

L-DKGPR vs. L-DKGPR-: We see a dramatic drop in regression performance when time-invariant effects are not modeled (L-DKGPR-) as compared to when they are (L-DKGPR). This underscores the importance of modeling the time-independent components of LC and CC for accurate modeling of longitudinal data. The decomposition of the correlation structure into the time-varying and time-invariant components simplifies this task. The time-invariant component is analogous to estimating the mean correlation whereas the time-varying component contributes to the residual. Hence, the decomposition of the correlation structure into the time-varying and time-invariant components should help reduce the variance of the estimated correlations.

L-DKGPR vs. L-RBF-GPR: L-DKGPR consistently outperforms L-RBF-GPR. The performance gap between L-DKGPR and L-RBF-GPR increases with the number of covariates. A possible explanation of this result has to do with the meaninglessness of Euclidean distance (and hence SE kernel) as a measure of similarity between data points in a high dimensional space [17]; and the ability of the learned deep kernel to map the data to a low-dimensional latent space where distances are meaningful.

5 Summary and Discussion

Summary. We have presented L-DKGPR, a novel longitudinal deep kernel Gaussian process regression model that overcomes some of the key limitations of existing state-of-the-art GP regression methods for predictive modeling from longitudinal data. To the best of our knowledge, L-DKGPR is the only method that fully automates the discovery of complex multi-level correlations from longitudinal data. L-DKGPR incorporates a deep kernel learning method that combines the expressive power of deep neural networks with the flexibility of non-parametric kernel methods, to automate the discovery of the complex multilevel correlation structure from longitudinal data. L-DKGPR uses a novel additive kernel that simultaneously accommodates both time-varying and the time-invariant effects. We have shown how L-DKGPR can be efficiently trained using inducing points in a low-dimensional latent space (as opposed to the data space) and the stochastic variational method. We report results of extensive experiments using both simulated and real-world benchmark longitudinal data sets that demonstrate the superior modeling accuracy as well as scalability of L-DKGPR over the state-of-the-art LDA methods. A case study with a real-world data set shows how the approach can be used to gain useful insights from longitudinal data.

Discussion. The inducing point methods play a crucial role in the design of L-DKGPR as they do in other sparse Gaussian Processes [25, 16]. The number of inducing points M provides a trade-off between approximation accuracy and efficiency. Therefore, determining the optimal choice of the number of inducing points remains an important but as yet open problem. Recent work [26] have shown that under some conditions, *i.e.*, input data are normally distributed and inducing points are drawn from a k -deterministic point process over K_{XX} with a squared exponential (SE) kernel, then as $N \rightarrow \infty$, $M = \mathcal{O}(\log^P N)$. We have empirically examined the number of inducing points needed for data sets with finite N , by comparing the regression performance with different M on simulated data. We find that when $M \geq 10$, the performance of L-DKGPR (as measured by R^2) is quite stable for *all* simulated data sets in our experiments.³ With $M = 10$ in *all of our experiments with simulated as well as real-world data*, L-DKGPR consistently outperforms the baseline methods. We conjecture that $M \approx \log N$ is a good choice for the number of latent space inducing points for L-DKGPR in practice, which is significantly smaller than the theoretical bound $\mathcal{O}(\log^P N)$ in [26] for $P > 1$. Proving or disproving this conjecture would require a deeper theoretical analysis of L-DKGPR.

³Details are provided in Appendix E.3.

Broader Impact

Longitudinal data are common in a broad range of applications, including health science, neurological research, social science, economic science, to name a few [1]. We have shown that our model is scalable and effective in handling longitudinal data that exhibits a priori unknown, complex correlation with minor or no efforts on tuning hyper-parameters.

Though our work is primarily motivated by the challenges exist in longitudinal data analysis, the proposed model preserves the flexibility to cope with any data that abide by or violate the independent and identically distributed (i.i.d.) assumption. In practice, our model can be directly applied to general regression, functional data, multivariate time series or spatio-temporal data. With mild modifications, our model can also be applied to structural data such as dynamic graphical data, where a finite set of nodes and/or edges between nodes are evolving over time. For example, one could encode the stationary (or non-stationary) edges between nodes with a new time-invariant (or time-varying) kernel by multiplying the corresponding deep kernel with a zero-sum kernel [12]. The advantage on using our model compared to the existing methods in these domains is that, in addition to delivering appealing prediction performance, our model offers rich longitudinal and cluster correlation structure that can be exploit to gain deeper insight towards the evolvement of variables, subject clustering and phase transitions, as well as prediction uncertainty over time (see Appendix 7 for example), which are considered important for evaluating the trustworthiness of the model predictions.

References

- [1] Hedeker, D., R. D. Gibbons. *Longitudinal data analysis*, vol. 451. John Wiley & Sons, 2006.
- [2] Gibbons, R. D., D. Hedeker. Random effects probit and logistic regression models for three-level data. *Biometrics*, pages 1527–1537, 1997.
- [3] Liang, J., D. Xu, Y. Sun, et al. Lmlfm: Longitudinal multi-level factorization machines. In *Proceedings of the AAAI Conference on Artificial Intelligence*, vol. 34. 2020.
- [4] Verbeke, G., S. Fieuws, G. Molenberghs, et al. The analysis of multivariate longitudinal data: A review. *Statistical methods in medical research*, 23(1):42–59, 2014.
- [5] Liang, K.-Y., S. L. Zeger. Longitudinal data analysis using generalized linear models. *Biometrika*, 73(1):13–22, 1986.
- [6] McCulloch, C. E. Maximum likelihood algorithms for generalized linear mixed models. *Journal of the American statistical Association*, 92(437):162–170, 1997.
- [7] Fitzmaurice, G. M., N. M. Laird, J. H. Ware. *Applied longitudinal analysis*, vol. 998. John Wiley & Sons, 2012.
- [8] Wang, M. Generalized estimating equations in longitudinal data analysis: a review and recent developments. *Advances in Statistics*, 2014, 2014.
- [9] Xiong, Y., H. J. Kim, V. Singh. Mixed effects neural networks (menets) with applications to gaze estimation. In *Proceedings of the IEEE Conference on Computer Vision and Pattern Recognition*, pages 7743–7752. 2019.
- [10] Quintana, F. A., W. O. Johnson, L. E. Waetjen, et al. Bayesian nonparametric longitudinal data analysis. *Journal of the American Statistical Association*, 111(515):1168–1181, 2016.
- [11] Cheng, L., S. Ramchandran, T. Vatanen, et al. An additive gaussian process regression model for interpretable non-parametric analysis of longitudinal data. *Nature communications*, 10(1):1798, 2019.
- [12] Timonen, J., H. Mannerström, A. Vehtari, et al. An interpretable probabilistic machine learning method for heterogeneous longitudinal studies. *arXiv preprint arXiv:1912.03549*, 2019.
- [13] Rasmussen, C. E. Gaussian processes in machine learning. In *Summer School on Machine Learning*, pages 63–71. Springer, 2003.
- [14] Wilson, A. G., Z. Hu, R. Salakhutdinov, et al. Deep kernel learning. In *Artificial Intelligence and Statistics*, pages 370–378. 2016.
- [15] Williams, C. K., C. E. Rasmussen. *Gaussian processes for machine learning*, vol. 2. MIT press Cambridge, MA, 2006.

- [16] Wilson, A. G., Z. Hu, R. R. Salakhutdinov, et al. Stochastic variational deep kernel learning. In *Advances in Neural Information Processing Systems*, pages 2586–2594, 2016.
- [17] Aggarwal, C. C., A. Hinneburg, D. A. Keim. On the surprising behavior of distance metrics in high dimensional space. In *International conference on database theory*, pages 420–434. Springer, 2001.
- [18] Goodfellow, I., Y. Bengio, A. Courville. *Deep learning*. MIT press, 2016.
- [19] Liu, H., Y.-S. Ong, X. Shen, et al. When gaussian process meets big data: A review of scalable gps. *IEEE Transactions on Neural Networks and Learning Systems*, 2020.
- [20] Sutton-Tyrrell, K., R. P. Wildman, K. A. Matthews, et al. Sex hormone-binding globulin and the free androgen index are related to cardiovascular risk factors in multiethnic premenopausal and perimenopausal women enrolled in the study of women across the nation (swan). *Circulation*, 111(10):1242–1249, 2005.
- [21] Smith, T., P. Marsden, M. Hout, et al. General social surveys, 1972–2014 [machine-readable data file]/principal investigator. *Sponsored by national science foundation. Chicago: National Opinion Research Center at the University of Chicago [producer and distributor]*, 2017.
- [22] Marinescu, R. V., N. P. Oxtoby, A. L. Young, et al. Tadpole challenge: Prediction of longitudinal evolution in alzheimer’s disease. *arXiv preprint arXiv:1805.03909*, 2018.
- [23] Bates, D., M. Mächler, B. Bolker, et al. Fitting linear mixed-effects models using lme4. *Journal of Statistical Software, Articles*, 67(1):1–48, 2015.
- [24] Inan, G., L. Wang. Pgee: An r package for analysis of longitudinal data with high-dimensional covariates. *R Journal*, 9(1):393–402, 2017.
- [25] Wilson, A., H. Nickisch. Kernel interpolation for scalable structured gaussian processes (kiss-gp). In *International Conference on Machine Learning*, pages 1775–1784, 2015.
- [26] Burt, D. R., C. E. Rasmussen, M. Van Der Wilk. Rates of convergence for sparse variational gaussian process regression. *arXiv preprint arXiv:1903.03571*, 2019.
- [27] Quiñero-Candela, J., C. E. Rasmussen. A unifying view of sparse approximate gaussian process regression. *Journal of Machine Learning Research*, 6(Dec):1939–1959, 2005.
- [28] Paszke, A., S. Gross, F. Massa, et al. Pytorch: An imperative style, high-performance deep learning library. In H. Wallach, H. Larochelle, A. Beygelzimer, F. d’Alché-Buc, E. Fox, R. Garnett, eds., *Advances in Neural Information Processing Systems 32*, pages 8024–8035. Curran Associates, Inc., 2019.
- [29] Barron, J. T. Continuously differentiable exponential linear units. *arXiv preprint arXiv:1704.07483*, 2017.
- [30] Radloff, L. S. The ces-d scale: A self-report depression scale for research in the general population. *Applied psychological measurement*, 1(3):385–401, 1977.

A. Derivations for L-DKGPR

Model Inference. We start with the ELBO:

$$\mathcal{L} \triangleq \mathbb{E}_{q(\mathbf{f}, \mathbf{u}|X, Z)} [\log p(\mathbf{y}|\mathbf{f})] - \text{KL}[q(\mathbf{u}|X, Z) || p(\mathbf{u}|Z)] \quad (11)$$

where $q(\mathbf{f}, \mathbf{u}|X, Z) = p(\mathbf{f}|\mathbf{u}, X, Z)q(\mathbf{u}|X, Z)$. Following the DTC assumption [19], we substitute $p(\mathbf{f}|\mathbf{u}, X, Z)$ with its deterministic form $\mathbf{f} = A\mathbf{u}$ with $A = K_{XZ}K_{ZZ}^{-1}$. Together with the reparameterization $q(\mathbf{u}|X, Z) = \boldsymbol{\mu}_q + L_q\boldsymbol{\epsilon}$ with $\boldsymbol{\epsilon} \sim \mathcal{N}(\mathbf{0}, I)$, we can rewrite the first term of (11) as:

$$\begin{aligned} \mathbb{E}_{q(\mathbf{f}, \mathbf{u}|X, Z)} [\log p(\mathbf{y}|\mathbf{f})] &= -N \log \sigma - \frac{1}{2\sigma^2} \mathbb{E}_{\boldsymbol{\epsilon} \sim \mathcal{N}(\mathbf{0}, I)} [(\mathbf{y} - A(\boldsymbol{\mu}_q + L_q\boldsymbol{\epsilon}))^\top (\mathbf{y} - A(\boldsymbol{\mu}_q + L_q\boldsymbol{\epsilon}))] \\ &= -N \log \sigma - \frac{1}{2\sigma^2} (\mathbf{y}^\top \mathbf{y} - 2\mathbf{y}^\top A\boldsymbol{\mu}_q + (A\boldsymbol{\mu}_q)^\top A\boldsymbol{\mu}_q + (AL_q\mathbf{1})^\top AL_q\mathbf{1}) \end{aligned} \quad (12)$$

Since the second term in (11) is the KL divergence between two multivariate Gaussian distributions, the analytical form can be obtained directly as

$$\text{KL}(q(\mathbf{u}|X, Z)||p(\mathbf{u}|Z)) = \frac{1}{2} \left[\log \frac{|K_{ZZ}|}{|L_q|^2} - M + \text{tr}(K_{ZZ}^{-1} L_q L_q^\top) + \boldsymbol{\mu}_q^\top K_{ZZ}^{-1} \boldsymbol{\mu}_q \right] \quad (13)$$

Combining (12) and (13), we therefore obtain:

$$\begin{aligned} \mathcal{L} = & \underbrace{-N \log \sigma - \frac{1}{2\sigma^2} (\mathbf{y}^\top \mathbf{y} - 2\mathbf{y}^\top A \boldsymbol{\mu}_q + (A \boldsymbol{\mu}_q)^\top A \boldsymbol{\mu}_q + (A L_q \mathbf{1})^\top A L_q \mathbf{1})}_{\mathbb{E}_{q(\mathbf{f}, \mathbf{u}|X, Z)}[\log p(\mathbf{y}|\mathbf{f})]} \\ & - \underbrace{\frac{1}{2} \left[\log \frac{|K_{ZZ}|}{|L_q|^2} - M + \text{tr}(K_{ZZ}^{-1} L_q L_q^\top) + \boldsymbol{\mu}_q^\top K_{ZZ}^{-1} \boldsymbol{\mu}_q \right]}_{\text{KL}[q(\mathbf{u}|X, Z)||p(\mathbf{u}|Z)]} \end{aligned} \quad (14)$$

where $\mathbf{1}$ is a column vector of ones. We can then compute the partial derivatives of \mathcal{L} w.r.t. the parameters of the proposal posterior $q(\mathbf{u}|X, Z)$ (i.e., $\{\boldsymbol{\mu}_q, L_q\}$) and derive its optimal form, such that:

$$\frac{\partial \mathcal{L}}{\partial \boldsymbol{\mu}_q} = \frac{1}{\sigma^2} (-A^\top \mathbf{y} + A^\top A \boldsymbol{\mu}_q) + K_{ZZ}^{-1} \boldsymbol{\mu}_q = 0 \quad (15)$$

$$\frac{\partial \mathcal{L}}{\partial L_q} = \frac{1}{\sigma^2} A^\top A L_q \mathbf{1} \mathbf{1}^\top + (L_q^{-\top} + K_{ZZ}^{-1} L_q) = 0 \quad (16)$$

Solving the above equations gives:

$$\boldsymbol{\mu}_q = \sigma^{-2} K_{ZZ} B K_{XZ}^\top \mathbf{y} \quad (17)$$

$$L_q (\mathbf{I} + \mathbf{1} \mathbf{1}^\top) = K_{ZZ} B K_{ZZ} \quad (18)$$

with $B = (K_{ZZ} + \sigma^{-2} K_{XZ}^\top K_{XZ})^{-1}$. To solve the triangular matrix L_q from (18), we first compute the Cholesky decomposition of $\mathbf{I} + \mathbf{1} \mathbf{1}^\top = C C^\top$ and $K_{ZZ} B K_{ZZ} = U U^\top$. We then simplify both side of (18) to $L_q C = U$. L_q can then be solved by exploiting the triangular structure on both side with

$$L_{i,i-k} = \frac{U_{i,i-k} - \sum_{j=0}^{k-1} L_{i,i-j} C_{i-j,i-k}}{C_{i-k,i-k}}, \quad k = 0, 1, \dots, i-1 \quad (19)$$

where $L_{i,j}$ is a short notation for $[L_q]_{i,j}$.

Prediction. A common approximation assumption associated with the inducing points idea is that the signals between training data and test data are conditionally independent given \mathbf{u} [27]. This is particularly useful during the test phase. Given the covariate matrix X_* for the test data, the prediction distribution is given by:

$$\begin{aligned} p(\mathbf{f}_* | X_*, X, y, Z) &= \int p(\mathbf{f}_*, \mathbf{f}, \mathbf{u} | X_*, X, y, Z) d\mathbf{f} d\mathbf{u} \\ &= \int p(\mathbf{f}_* | \mathbf{u}, X_*, Z) p(\mathbf{f}, \mathbf{u} | X, y, Z) d\mathbf{f} d\mathbf{u} \\ &\simeq \mathbb{E}_{q(\mathbf{u}|X, Z)} [p(\mathbf{f}_* | \mathbf{u}, X_*, Z)] \\ &= \mathcal{N}(K_{X_*Z} [K_{ZZ} + \sigma^2 \mathbf{I}]^{-1} \boldsymbol{\mu}_q, K_{X_*X_*} - K_{X_*Z} [K_{ZZ} + \sigma^2 \mathbf{I}]^{-1} K_{X_*Z}^\top) \end{aligned} \quad (20)$$

We can then make prediction using the mode and evaluate the prediction uncertainty with the covariance matrix from (20).

B. L-DKGPR Algorithm

We separate the model parameters into two groups, i.e., parameters w.r.t. the proposal posterior $\{\boldsymbol{\mu}_q, L_q\}$ and the remaining parameters Θ , and use an EM-like algorithm to update both groups alternatively. The L-DKGPR algorithm is listed in Algorithm 1.

Algorithm 1: L-DKGPR

Input: Training set $S = \{X, \mathbf{y}\}$, latent dimension D_v, D_i , number of inducing points M , gradient-based optimizer and its related hyper-parameters (*i.e.*, learning rate, weight decay, mini-batch size), alternating frequency T .

// See Section D for details.

Output: The learned L-DKGPR model.

```
1 Initialize the parameters  $\Theta = \{\sigma^2, Z, \alpha^{(v)}, \alpha^{(i)}, \gamma, \phi\}$ 
2 while Not converged do
3   Update proposal posterior  $q(\mathbf{u}|X, Z)$  according to (17) and (19)
4    $t = 0$ 
5   for  $t < T$  do
6     Update  $\Theta$  using the input optimizer.
7      $t = t + 1$ 
```

C. Implementation Details and Parameter Setup

We implement L-DKGPR using PyTorch [28]. We formulate e_γ using a deep neural network (DNN) consisting of multiple fully connected layers. Specifically, the structure of e_γ is P - H -CELU-Dropout(0.2)- H -CELU-Dropout(0.2)- D_v , where H is the size of hidden units and CELU stands for Continuously Differentiable Exponential Linear Units [29]. We set $H = 16$ for simulated data and $H = 32$ for real-life data. The latent dimension D_v is fixed at 10 for all experiments. Although we only use a simple fully connected structure throughout the experiment, the implementation is flexible enough to allow more advanced DNN structure such as CNN and RNN. The embedding function g_ϕ is a I -by- D_i parameter matrix. We set $D_i = D_v$. Though the full lower triangular matrix L_q can be computed using (19), we find that approximating L_q by using only its main diagonal components provides similar accuracy, but have substantially less computation and numerically stable. Therefore, in our implementation, $\tilde{L}_q = \text{diag}(U/C)$. We update $\Theta = \{\sigma^2, Z, \alpha^{(v)}, \alpha^{(i)}, \gamma, \phi\}$ using Adam optimizer. The learning rate for $\Theta - \{\phi\}$ is fixed at 0.001. To facilitate more effective learning on cluster correlation, we assign larger learning rate on $\{\phi\}$, which is fixed at 0.01. The training and testing batch sizes are set to 1024. The maximum training epoch of L-DKGPR is set to 300 for all data sets. We use early stopping if the R^2 evaluated on validation set decrease in two consecutive epochs. The number of Inducing points is fixed at 10 for all data sets. We initialize $\{\sigma^2, \alpha^{(v)}, \alpha^{(i)}\} = 1$, $Z \sim U[0, 1)^{M \times (D_v + D_i)}$. γ, ϕ are initialized with the default initialization mechanism in PyTorch. To avoid numerical issue during Cholesky decomposition, we add a small factor $\Delta = \text{diag}(\mathbf{0.001})$ to the main diagonal of the correlation matrix.

As for the implementation of our baseline methods, we use the implementations of GLMM, GEE and LGPR available in the `lmer4`, `PGEE` and `lgpr` packages, respectively from CRAN.⁴ We use the LMLFM implementation from <https://github.com/junjieliang672/LMLFM>. For GLMM, we keep most hyper-parameters to their default values but increase the maximum iteration to 200. In GEE, we use an first-order auto-regressive correlation structure. The maximum iteration is fixed at 200. For LGPR, results are averaged over 5 independent simulated chains. For each chain, we use 2000 iterations. The number of burn-in samples is fixed at 200.

All experiments are conducted on a desktop machine with Intel Core i7-7700K CPU, 16GB RAM and GTX 1060 6GB graphics card. Codes are available through <https://anonymous.4open.science/r/cce1f2c6-29ff-4941-993d-d597a71ecc8c/>.

D. Experimental Data Setup

Generating Simulated Data. We construct simulated longitudinal data sets that exhibit *i.e.*, longitudinal correlation (LC) and multilevel correlation (MC) as follows: The outcome is generated using $\mathbf{y} = f(X) + \epsilon$ where $f(X)$ is a non-linear transformation based on the observed

⁴<https://cran.r-project.org/>

Table 4: Runtime (in second) comparison on real-world data sets. We use ‘N/A’ to denote execution error.

Data sets	N	I	P	L-DKGPR	LGPR	LMLFM	GLMM	GEE
TADPOLE	595	50	24	0.03	6.39	0.01	0.01	0.13
SWAN	550	50	137	0.03	26.1	0.02	0.06	0.59
GSS	1,500	50	1,553	0.12	N/A	0.30	N/A	30.1
TADPOLE	8,771	1,681	24	1.48	N/A	0.25	0.03	4.66
SWAN	28,405	3,300	137	4.48	N/A	1.74	N/A	N/A
GSS	59,599	4,510	1,553	5.31	N/A	24.35	N/A	N/A

covariate matrix X and the residual $\epsilon \sim N(\mathbf{0}, \Sigma)$. To simulate longitudinal correlation, we simply set Σ to a block diagonal matrix. For each individual, we use a first-order auto-regressive correlation structure (AR(1)) with decaying factor fixed at 0.9. To simulate a data set that exhibits multilevel correlation, we first split the individuals into C clusters. We then define the cluster correlation matrix by setting the correlation associated to data points in the same cluster to 1. Finally, we compute the multilevel correlation by summing up the longitudinal correlation and cluster correlation. Following [11, 12], we simulate 40 individuals, 20 observations, and 30 covariates for each individual. To simulate correlation among the covariates, we first generate 10 base features independently from $[0, 1]$ uniform distribution, then the covariate matrix X is computed using an encoder network with architecture $10 - 100 - \text{Tanh} - \text{Dropout}(0.7) - \text{BatchNorm} - 30 - \text{Tanh}$. It therefore results in 30 covariates that are conditionally independent given encoder network and base features. We hold out both the base features and the encoder network to all comparing methods, thus leading to a covariate matrix with non-linear correlation that is unknown to all methods. To generate \mathbf{y} , we use another nonlinear transformation $f(X)$, which is defined by a network with structure $30 - 100 - \text{Tanh} - 1$. In our experiment, We vary the number of clusters C from [2, 5].

Pre-processing on SWAN data. Since CESD score is not contained from the original SWAN data, we manually compute the score based on its definition [30]. To form the outcome label, we define an adjusted CESD score by $y = \text{CESD} - 15$, thus $y \geq 0$ indicates depression. We center \mathbf{y} with $\mathbf{y} = \mathbf{y} - \text{mean}(\mathbf{y})$. After computing the label, we exclude all columns that are directly associated to computing the CESD score. We convert the categorical features using one-hot encoding and perform standard scaling on the continuous features.

Pre-processing on GSS data. Since the original data set contains repeated columns for the same survey question, we keep only one column for each survey question. We re-format all the answer codes associated to ‘unknown’ and ‘missing’ to ‘unknown’. The outcome label is derived from the field ‘General Happiness’, we code the value ‘pretty happen’ and ‘very happy’ to 1 and the others to -1 . As the other covariates, We convert the categorical features using one-hot encoding and perform standard scaling on the continuous features.

Pre-processing on TADPOLE data. There are three data sets in the original files. We first combine the three data sets and remove the repeated data points. Then, we convert the categorical features using one-hot encoding and perform standard scaling on the continuous features. The outcome label is defined by the value of ‘ADAS13’. Similarly, we center the label with $\mathbf{y} = \mathbf{y} - \text{mean}(\mathbf{y})$.

E. Additional Experiment Results

E.1. Run time Comparison

The CPU run times and failure to complete execution on the real-world data sets are reported in 4. We see that LGPR, GLMM and GEE are exceptionally sensitive to the number of variables. Indeed, their computational complexity increases proportional to P^3 where P is the number of variables. In contrast, L-DKGPR and LMLFM scale gracefully with increase in the number of individuals as well as the number of variables in the data set.

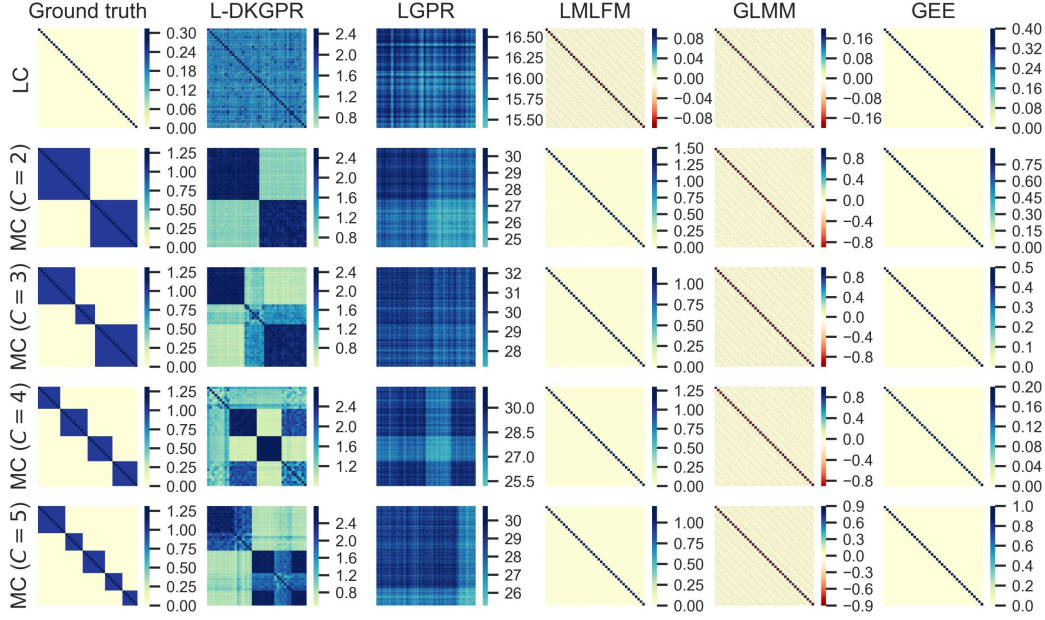


Figure 3: Outcome correlation estimated by all methods on simulated data.

E.2. More on (RQ3): Can L-DKGPR reliably recover the rich correlation structure from the data?

Correction Structure in Simulated Data.

The outcome correlations estimated by all methods on the simulated data are shown in Figure 3. It is easy to see that LMLFM, GLMM and GEE are incapable of recovering MC. Though LGPR can, model data which exhibit MC, the resulting correlation is overly simple. In the presence of MC with $C > 2$, we see that only one known cluster is correctly recovered. We conjecture that the inferior performance of LGPR is due to the limited expressive power of the kernel functions it used. We note that L-GKDPR is able to recover most of the correlation structure present in the data. We further note that L-DKGPR, despite being the best performer among the methods compared in this study, it tends to underestimate the number of clusters because the full data correlation is approximated by a low-rank matrix (see Eq. (20)) resulting in information loss.

Correlation Structure in Real-World Data. We show how the correlation structure discovered by L-DKGPR can offer useful insights into longitudinal data gathered in real-world settings. Because of space constraints, we only analyze the correlation structure uncovered by L-DKGPR from the SWAN data.

Figure 4(a) displays the time-invariant cluster correlation after fitting the model to the full SWAN data. We find that the individuals can be roughly grouped into two clusters of which the first shows a clear cluster structure. The distributions of the adjusted CESD score of the two clusters are presented in Figure 4(b). We find that individuals assigned to cluster #1 tend to have lower risk of depression whereas those assigned to cluster #2 tend to have higher risk of depression. Closer examination of individuals assigned to the clusters reveals potentially useful suggestions for further analysis. In our case study, we can identify at least two individuals stand out for further in-depth investigation (See Figure 5). **Individual #1:** Judging from the longitudinal correlation as shown in Figure 5(a), we detect a clear transition from non-depression to depression starting around age 52. Comparison of the covariates between age 52 and 53 reveals potential reasons for the transition e.g., having family and financial issues at 53 that were not present before age 52. In addition, while we have two observations at the age of 55, the first observation tends to be uncorrelated with the others, and hence more likely to be an outlier. Another interesting finding is that, although our model detects a potential transition from non-depression to depression, the predictions are consistently below the threshold, making the

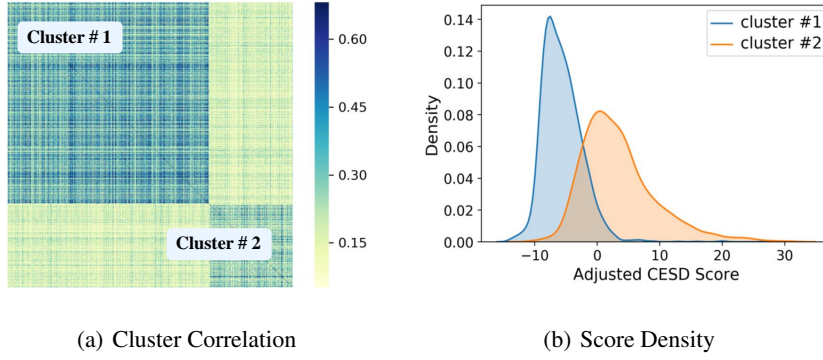


Figure 4: Cluster correlation analysis on SWAN Data. (a) We find that individuals can be roughly split into two clusters; (b) Adjusted CESD score density for the two clusters.

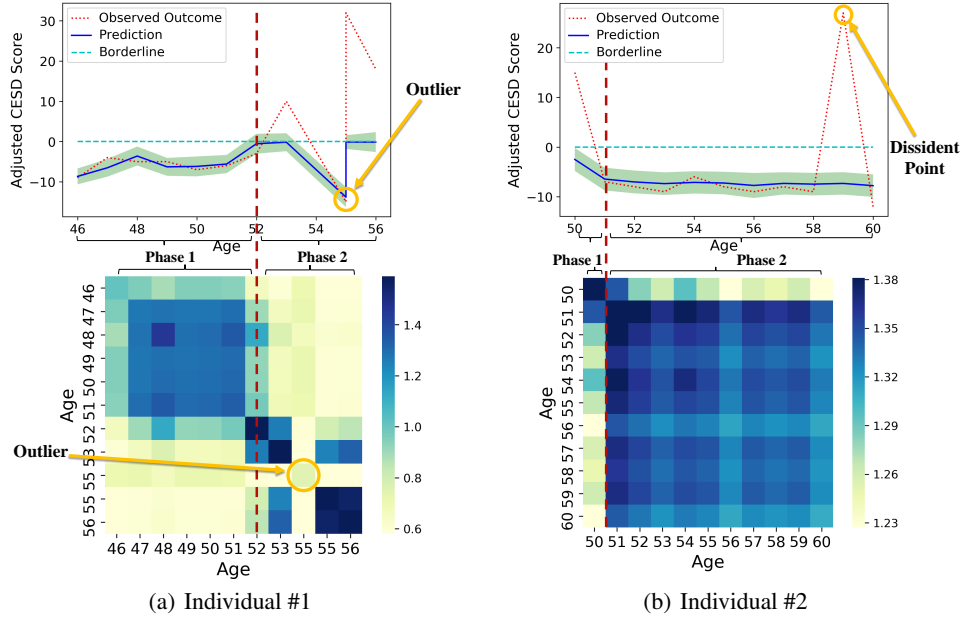


Figure 5: Case study for two selected individuals from cluster #1. (Top figures) Observed and predicted trajectories for the adjusted CESD scores; (Bottom figures) Longitudinal correlation among the predictions.

individual non-depressive overall. This could further imply that the depression symptom associated with individual #1 is on mild and could be temporary. Perhaps mental health services could help individual #1 to successfully get through what appears to be a temporary depression, likely triggered by family and financial issues. **Individual #2:** In the case of individual #2 shown in Figure 5(b) we find a transition from non-depression to depression around age 50. The transition is perhaps explained by fact that individual #2 is going through a change of menopausal status between age of 50 and 51. It is worth noting that a sudden rise in CESD score is observed at the age of 59 (the dissident point), which, surprisingly, is consistently ignored by our model. To understand why, we search for clues by comparing the covariates between age of 58, 59 and 60. Results turn out that no clear evidence are found to support the sudden depression. Therefore, we conjecture that the observed adjusted CESD score at 59 is likely unreliable and a more careful examination might have been warranted. In summary, the correlation structure revealed by L-DKGPR offers useful insights into longitudinal data.

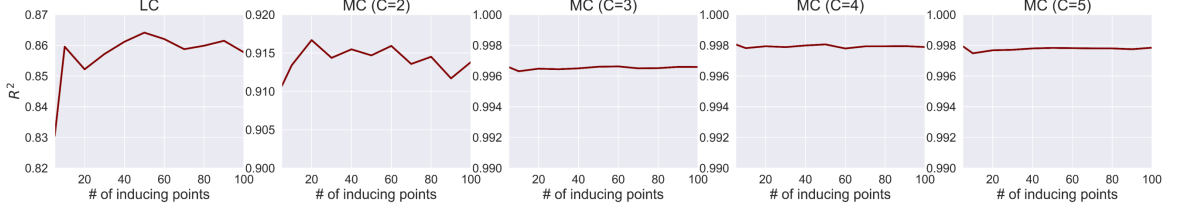


Figure 6: Regression performance with different numbers of inducing points on simulated data.

E.3. How does the number of inducing points M affects the overall performance of L-DKGPR?

The number of inducing points provides a trade-off between approximation accuracy and efficiency in sparse GP methods. In this experiment, we vary the number of inducing points from 5 – 100 on simulated data and record the R^2 as shown in Figure 6. We find that when the number of inducing points is above a certain threshold, *i.e.*, 10 in *all* simulated settings, the regression performance is rather stable regardless the increasing of inducing points. A theoretical study [26] points out that when input data are normally distributed and inducing points are drawn from a k -deterministic point process (k -DPP) over K_{XX} with an SE-ARD kernel, then as $N \rightarrow \infty$, $M = \mathcal{O}(\log^P N)$ where P is the input dimension. In our case, if we treat the latent representation as the input dimension as considered in [26], then the number of inducing points suffice to our simulated data should be $M = \log^{10}(1600)$, which is unacceptably large. In contrast, we empirically show that $M \approx \log N$ is sufficient to get appealing results. We conjecture that this is because instead of drawing the inducing points from a k -DPP process from the input data, we optimize representation of the inducing points jointly with the other model parameters, thus delivering more effective inducing points that summarize the variance of the input data.

Supplementary Material: Longitudinal Deep Kernel Gaussian Process Regression

Anonymous Author(s)

Affiliation

Address

email

1 A Derivations for L-DKGPR

2 **Model Inference.** We start with the ELBO:

$$\mathcal{L} \triangleq \mathbb{E}_{q(\mathbf{f}, \mathbf{u}|X, Z)} [\log p(\mathbf{y}|\mathbf{f})] - \text{KL}[q(\mathbf{u}|X, Z)||p(\mathbf{u}|Z)] \quad (1)$$

3 where $q(\mathbf{f}, \mathbf{u}|X, Z) = p(\mathbf{f}|\mathbf{u}, X, Z)q(\mathbf{u}|X, Z)$. Following the DTC assumption [?], we substitute
 4 $p(\mathbf{f}|\mathbf{u}, X, Z)$ with its deterministic form $\mathbf{f} = A\mathbf{u}$ with $A = K_{XZ}K_{ZZ}^{-1}$. Together with the reparam-
 5 terization $q(\mathbf{u}|X, Z) = \boldsymbol{\mu}_q + L_q\boldsymbol{\epsilon}$ with $\boldsymbol{\epsilon} \sim \mathcal{N}(\mathbf{0}, I)$, we can rewrite the first term of (1) as:

$$\begin{aligned} \mathbb{E}_{q(\mathbf{f}, \mathbf{u}|X, Z)} [\log p(\mathbf{y}|\mathbf{f})] &= -N \log \sigma - \frac{1}{2\sigma^2} \mathbb{E}_{\boldsymbol{\epsilon} \sim \mathcal{N}(\mathbf{0}, I)} [(\mathbf{y} - A(\boldsymbol{\mu}_q + L_q\boldsymbol{\epsilon}))^\top (\mathbf{y} - A(\boldsymbol{\mu}_q + L_q\boldsymbol{\epsilon}))] \\ &= -N \log \sigma - \frac{1}{2\sigma^2} (\mathbf{y}^\top \mathbf{y} - 2\mathbf{y}^\top A\boldsymbol{\mu}_q + (A\boldsymbol{\mu}_q)^\top A\boldsymbol{\mu}_q + (AL_q\mathbf{1})^\top AL_q\mathbf{1}) \end{aligned} \quad (2)$$

6 Since the second term in (1) is the KL divergence between two multivariate Gaussian distributions,
 7 the analytical form can be obtained directly as

$$\text{KL}(q(\mathbf{u}|X, Z)||p(\mathbf{u}|Z)) = \frac{1}{2} \left[\log \frac{|K_{ZZ}|}{|L_q|^2} - M + \text{tr}(K_{ZZ}^{-1}L_qL_q^\top) + \boldsymbol{\mu}_q^\top K_{ZZ}^{-1}\boldsymbol{\mu}_q \right] \quad (3)$$

8 Combining (2) and (3), we therefore obtain:

$$\begin{aligned} \mathcal{L} &= \underbrace{-N \log \sigma - \frac{1}{2\sigma^2} (\mathbf{y}^\top \mathbf{y} - 2\mathbf{y}^\top A\boldsymbol{\mu}_q + (A\boldsymbol{\mu}_q)^\top A\boldsymbol{\mu}_q + (AL_q\mathbf{1})^\top AL_q\mathbf{1})}_{\mathbb{E}_{q(\mathbf{f}, \mathbf{u}|X, Z)} [\log p(\mathbf{y}|\mathbf{f})]} \\ &\quad - \underbrace{\frac{1}{2} \left[\log \frac{|K_{ZZ}|}{|L_q|^2} - M + \text{tr}(K_{ZZ}^{-1}L_qL_q^\top) + \boldsymbol{\mu}_q^\top K_{ZZ}^{-1}\boldsymbol{\mu}_q \right]}_{\text{KL}[q(\mathbf{u}|X, Z)||p(\mathbf{u}|Z)]} \end{aligned} \quad (4)$$

9 where $\mathbf{1}$ is a column vector of ones. We can then compute the partial derivatives of \mathcal{L} w.r.t. the
 10 parameters of the proposal posterior $q(\mathbf{u}|X, Z)$ (i.e., $\{\boldsymbol{\mu}_q, L_q\}$) and derive its optimal form, such
 11 that:

$$\frac{\partial \mathcal{L}}{\partial \boldsymbol{\mu}_q} = \frac{1}{\sigma^2} (-A^\top \mathbf{y} + A^\top A\boldsymbol{\mu}_q) + K_{ZZ}^{-1}\boldsymbol{\mu}_q = 0 \quad (5)$$

$$\frac{\partial \mathcal{L}}{\partial L_q} = \frac{1}{\sigma^2} A^\top AL_q\mathbf{1}\mathbf{1}^\top + (L_q^{-\top} + K_{ZZ}^{-1}L_q) = 0 \quad (6)$$

Algorithm 1: L-DKGPR

Input: Training set $S = \{X, \mathbf{y}\}$, latent dimension D_v, D_i , number of inducing points M , gradient-based optimizer and its related hyper-parameters (*i.e.*, learning rate, weight decay, mini-batch size), alternating frequency T .

// See Section D for details.

Output: The learned L-DKGPR model.

```
1 Initialize the parameters  $\Theta = \{\sigma^2, Z, \alpha^{(v)}, \alpha^{(i)}, \gamma, \phi\}$ 
2 while Not converged do
3   Update proposal posterior  $q(\mathbf{u}|X, Z)$  according to (7) and (9)
4    $t = 0$ 
5   for  $t < T$  do
6     Update  $\Theta$  using the input optimizer.
7      $t = t + 1$ 
```

12 Solving the above equations gives:

$$\boldsymbol{\mu}_q = \sigma^{-2} K_{ZZ} B K_{XZ}^\top \mathbf{y} \quad (7)$$

$$L_q (\mathbf{I} + \mathbf{1}\mathbf{1}^\top) = K_{ZZ} B K_{ZZ} \quad (8)$$

13 with $B = (K_{ZZ} + \sigma^{-2} K_{XZ}^\top K_{XZ})^{-1}$. To solve the triangular matrix L_q from (8), we first compute
14 the Cholesky decomposition of $\mathbf{I} + \mathbf{1}\mathbf{1}^\top = CC^\top$ and $K_{ZZ} B K_{ZZ} = UU^\top$. We then simplify both
15 side of (8) to $L_q C = U$. L_q can then be solved by exploiting the triangular structure on both side
16 with

$$L_{i,i-k} = \frac{U_{i,i-k} - \sum_{j=0}^{k-1} L_{i,i-j} C_{i-j,i-k}}{C_{i-k,i-k}}, \quad k = 0, 1, \dots, i-1 \quad (9)$$

17 where $L_{i,j}$ is a short notation for $[L_q]_{i,j}$.

18 **Prediction.** A common approximation assumption associated with the inducing points idea is that
19 the signals between training data and test data are conditionally independent given \mathbf{u} [?]. This is
20 particularly useful during the test phase. Given the covariate matrix X_* for the test data, the prediction
21 distribution is given by:

$$\begin{aligned} p(\mathbf{f}_* | X_*, X, y, Z) &= \int p(\mathbf{f}_*, \mathbf{f}, \mathbf{u} | X_*, X, y, Z) d\mathbf{f} d\mathbf{u} \\ &= \int p(\mathbf{f}_* | \mathbf{u}, X_*, Z) p(\mathbf{f}, \mathbf{u} | X, y, Z) d\mathbf{f} d\mathbf{u} \\ &\simeq \mathbb{E}_{q(\mathbf{u}|X,Z)} [p(\mathbf{f}_* | \mathbf{u}, X_*, Z)] \\ &= \mathcal{N}(K_{X_*Z} [K_{ZZ} + \sigma^2 \mathbf{I}]^{-1} \boldsymbol{\mu}_q, K_{X_*X_*} - K_{X_*Z} [K_{ZZ} + \sigma^2 \mathbf{I}]^{-1} K_{X_*Z}^\top) \end{aligned} \quad (10)$$

22 We can then make prediction using the mode and evaluate the prediction uncertainty with the
23 covariance matrix from (10).

24 B L-DKGPR Algorithm

25 We separate the model parameters into two groups, *i.e.*, parameters w.r.t. the proposal posterior
26 $\{\boldsymbol{\mu}_q, L_q\}$ and the remaining parameters Θ , and use an EM-like algorithm to update both groups
27 alternatively. The L-DKGPR algorithm is listed in Algorithm 1.

28 C Implementation Details and Parameter Setup

29 We implement L-DKGPR using PyTorch [?]. We formulate e_γ using a deep neural net-
30 work (DNN) consisting of multiple fully connected layers. Specifically, the structure of e_γ is
31 P - H -CELU-Dropout(0.2)- H -CELU-Dropout(0.2)- D_v , where H is the size of hidden units

and CELU stands for Continuously Differentiable Exponential Linear Units [?]. We set $H = 16$ for simulated data and $H = 32$ for real-life data. The latent dimension D_v is fixed at 10 for all experiments. Although we only use a simple fully connected structure throughout the experiment, the implementation is flexible enough to allow more advanced DNN structure such as CNN and RNN. The embedding function g_ϕ is a I -by- D_i parameter matrix. We set $D_i = D_v$. Though the full lower triangular matrix L_q can be computed using (9), we find that approximating L_q by using only its main diagonal components provides similar accuracy, but have substantially less computation and numerically stable. Therefore, in our implementation, $\tilde{L}_q = \text{diag}(U/C)$. We update $\Theta = \{\sigma^2, Z, \alpha^{(v)}, \alpha^{(i)}, \gamma, \phi\}$ using Adam optimizer. The learning rate for $\Theta - \{\phi\}$ is fixed at 0.001. To facilitate more effective learning on cluster correlation, we assign larger learning rate on $\{\phi\}$, which is fixed at 0.01. The training and testing batch sizes are set to 1024. The maximum training epoch of L-DKGPR is set to 300 for all data sets. We use early stopping if the R^2 evaluated on validation set decrease in two consecutive epochs. The number of Inducing points is fixed at 10 for all data sets. We initialize $\{\sigma^2, \alpha^{(v)}, \alpha^{(i)}\} = 1$, $Z \sim U[0, 1)^{M \times (D_v + D_i)}$. γ, ϕ are initialized with the default initialization mechanism in PyTorch. To avoid numerical issue during Cholesky decomposition, we add a small factor $\Delta = \text{diag}(\mathbf{0.001})$ to the main diagonal of the correlation matrix.

As for the implementation of our baseline methods, we use the implementations of GLMM, GEE and LGPR available in the `lmer4`, `PGEE` and `lgpr` packages, respectively from CRAN.¹. We use the LMLFM implementation from <https://github.com/junjieliang672/LMLFM>. For GLMM, we keep most hyper-parameters to their default values but increase the maximum iteration to 200. In GEE, we use an first-order auto-regressive correlation structure. The maximum iteration is fixed at 200. For LGPR, results are averaged over 5 independent simulated chains. For each chain, we use 2000 iterations. The number of burn-in samples is fixed at 200.

All experiments are conducted on a desktop machine with Intel Core i7-7700K CPU, 16GB RAM and GTX 1060 6GB graphics card. Codes are available through <https://anonymous.4open.science/r/cce1f2c6-29ff-4941-993d-d597a71ecc8c/>.

D Experimental Data Setup

Generating Simulated Data. We construct simulated longitudinal data sets that exhibit *i.e.*, longitudinal correlation (LC) and multilevel correlation (MC) as follows: The outcome is generated using $\mathbf{y} = f(X) + \epsilon$ where $f(X)$ is a non-linear transformation based on the observed covariate matrix X and the residual $\epsilon \sim N(\mathbf{0}, \Sigma)$. To simulate longitudinal correlation, we simply set Σ to a block diagonal matrix. For each individual, we use a first-order auto-regressive correlation structure (AR(1)) with decaying factor fixed at 0.9. To simulate a data set that exhibits multilevel correlation, we first split the individuals into C clusters. We then define the cluster correlation matrix by setting the correlation associated to data points in the same cluster to 1. Finally, we compute the multilevel correlation by summing up the longitudinal correlation and cluster correlation. Following [?, ?], we simulate 40 individuals, 20 observations, and 30 covariates for each individual. To simulate correlation among the covariates, we first generate 10 base features independently from $[0, 1)$ uniform distribution, then the covariate matrix X is computed using an encoder network with architecture $10 - 100 - \text{Tanh} - \text{Dropout}(0.7) - \text{BatchNorm} - 30 - \text{Tanh}$. It therefore results in 30 covariates that are conditionally independent given encoder network and base features. We hold out both the base features and the encoder network to all comparing methods, thus leading to a covariate matrix with non-linear correlation that is unknown to all methods. To generate \mathbf{y} , we use another nonlinear transformation $f(X)$, which is defined by a network with structure $30 - 100 - \text{Tanh} - 1$. In our experiment, We vary the number of clusters C from [2, 5].

Pre-processing on SWAN data. Since CESD score is not contained from the original SWAN data, we manually compute the score based on its definition [?]. To form the outcome label, we define an adjusted CESD score by $y = \text{CESD} - 15$, thus $y \geq 0$ indicates depression. We center \mathbf{y} with $\mathbf{y} = \mathbf{y} - \text{mean}(\mathbf{y})$. After computing the label, we exclude all columns that are directly associated to

¹<https://cran.r-project.org/>

Table 1: Runtime (in second) comparison on real-world data sets. We use ‘N/A’ to denote execution error.

Data sets	N	I	P	L-DKGPR	LGPR	LMLFM	GLMM	GEE
TADPOLE	595	50	24	0.03	6.39	0.01	0.01	0.13
SWAN	550	50	137	0.03	26.1	0.02	0.06	0.59
GSS	1,500	50	1,553	0.12	N/A	0.30	N/A	30.1
TADPOLE	8,771	1,681	24	1.48	N/A	0.25	0.03	4.66
SWAN	28,405	3,300	137	4.48	N/A	1.74	N/A	N/A
GSS	59,599	4,510	1,553	5.31	N/A	24.35	N/A	N/A

82 computing the CESD score. We convert the categorical features using one-hot encoding and perform
83 standard scaling on the continuous features.

84 **Pre-processing on GSS data.** Since the original data set contains repeated columns for the same
85 survey question, we keep only one column for each survey question. We re-format all the answer
86 codes associated to ‘unknown’ and ‘missing’ to ‘unknown’. The outcome label is derived from the
87 field ‘General Happiness’, we code the value ‘pretty happen’ and ‘very happy’ to 1 and the others to
88 -1 . As the other covaraites, We convert the categorical features using one-hot encoding and perform
89 standard scaling on the continuous features.

90 **Pre-processing on TADPOLE data.** There are three data sets in the original files. We first combine
91 the three data sets and remove the repeated data points. Then, we convert the categorical features
92 using one-hot encoding and perform standard scaling on the continuous features. The outcome label
93 is defined by the value of ‘ADAS13’. Similarly, we center the label with $y = y - \text{mean}(y)$.

94 E Additional Experiment Results

95 E.1 Run time Comparison

96 The CPU run times and failure to complete execution on the real-world data sets are reported in 1.
97 We see that LGPR, GLMM and GEE are exceptionally sensitive to the number of variables. Indeed,
98 their computational complexity increases proportional to P^3 where P is the number of variables. In
99 contrast, L-DKGPR and LMLFM scale gracefully with increase in the number of individuals as well
100 as the number of variables in the data set.

101 E.2 More on (RQ3): Can L-DKGPR reliably recover the rich correlation structure from the 102 data?

103 Correction Structure in Simulated Data.

104 The outcome correlations estimated by all methods on the simulated data are shown in Figure 1. It
105 is easy to see that LMLFM, GLMM and GEE are incapable of recovering MC. Though LGPR can,
106 model data which exhibit MC, the resulting correlation is overly simple. In the presence of MC with
107 $C > 2$, we see that only one known cluster is correctly recovered. We conjecture that the inferior
108 performance of LGPR is due to the limited expressive power of the kernel functions it used. We note
109 that L-GKDPR is able to recover most of the correlation structure present in the data. We further
110 note that L-DKGPR, despite being the best performer among the methods compared in this study, it
111 tends to underestimate the number of clusters because the full data correlation is approximated by a
112 low-rank matrix (see Eq. (10)) resulting in information loss.

113 **Correlation Structure in Real-World Data.** We show how the correlation structure discovered by
114 L-DKGPR can offer useful insights into longitudinal data gathered in real-world settings. Because of
115 space constraints, we only analyze the correlation structure uncovered by L-DKGPR from the SWAN
116 data.

117 Figure 2(a) displays the time-invariant cluster correlation after fitting the model to the full SWAN
118 data. We find that the individuals can be roughly grouped into two clusters of which the first shows a

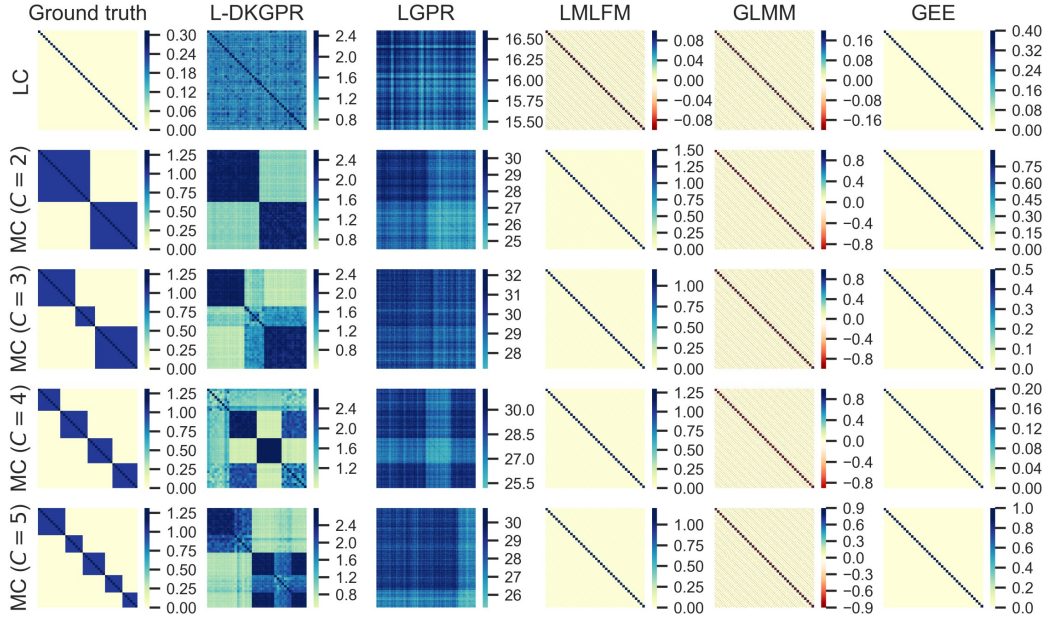


Figure 1: Outcome correlation estimated by all methods on simulated data.

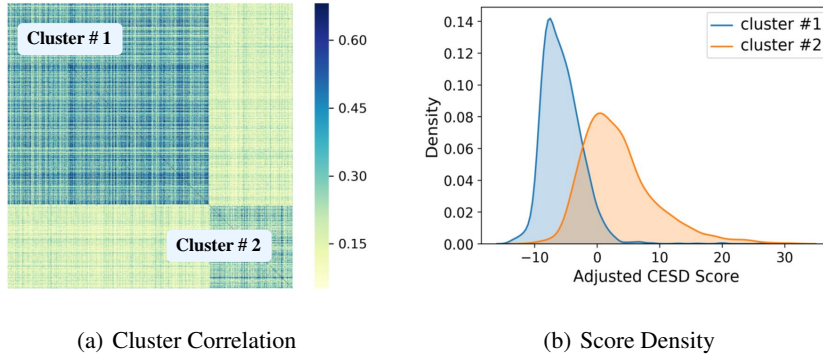


Figure 2: Cluster correlation analysis on SWAN Data. (a) We find that individuals can be roughly split into two clusters; (b) Adjusted CESD score density for the two clusters.

clear cluster structure. The distributions of the adjusted CESD score of the two clusters are presented in Figure 2(b). We find that individuals assigned to cluster #1 tend to have lower risk of depression whereas those assigned to cluster #2 tend to have higher risk of depression. Closer examination of individuals assigned to the clusters reveals potentially useful suggestions for further analysis. In our case study, we can identify at least two individuals stand out for further in-depth investigation (See Figure 3). **Individual #1:** Judging from the longitudinal correlation as shown in Figure 3(a), we detect a clear transition from non-depression to depression starting around age 52. Comparison of the covariates between age 52 and 53 reveals potential reasons for the transition e.g., having family and financial issues at 53 that were not present before age 52. In addition, while we have two observations at the age of 55, the first observation tends to be uncorrelated with the others, and hence more likely to be an outlier. Another interesting finding is that, although our model detects a potential transition from non-depression to depression, the predictions are consistently below the threshold, making the individual non-depressive overall. This could further imply that the depression symptom associated with individual #1 is on mild and could be temporary. Perhaps mental health services could help individual #1 to successfully get through what appears to be a temporary depression, likely triggered by family and financial issues. **Individual #2:** In the case of individual #2 shown in Figure 3(b) we

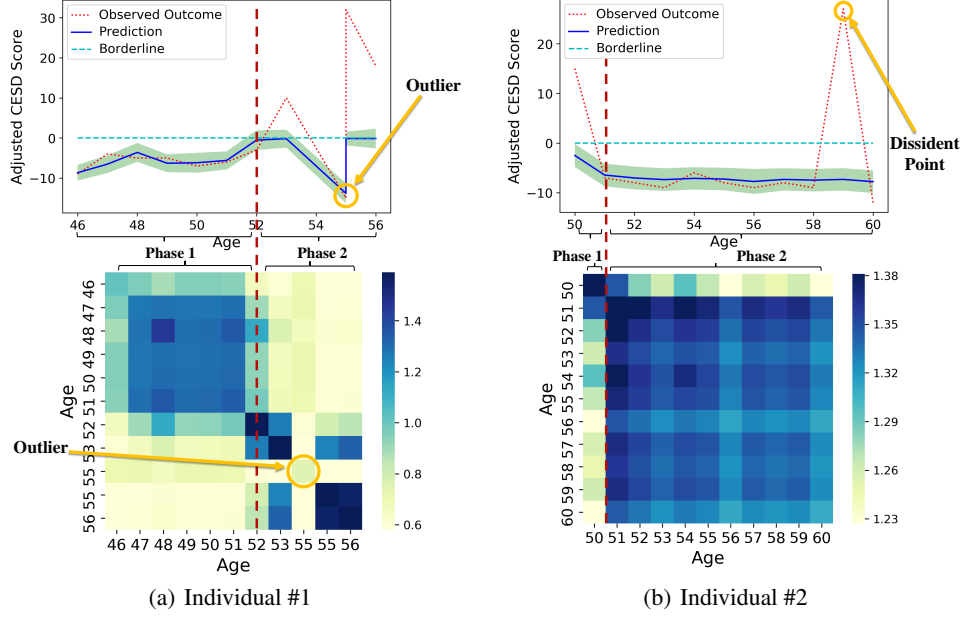


Figure 3: Case study for two selected individuals from cluster #1. (Top figures) Observed and predicted trajectories for the adjusted CESD scores; (Bottom figures) Longitudinal correlation among the predictions.

find a transition from non-depression to depression around age 50. The transition is perhaps explained by fact that individual #2 is going through a change of menopausal status between age of 50 and 51. It is worth noting that a sudden rise in CESD score is observed at the age of 59 (the dissident point), which, surprisingly, is consistently ignored by our model. To understand why, we search for clues by comparing the covariates between age of 58, 59 and 60. Results turn out that no clear evidence are found to support the sudden depression. Therefore, we conjecture that the observed adjusted CESD score at 59 is likely unreliable and a more careful examination might have been warranted. In summary, the correlation structure revealed by L-DKGPR offers useful insights into longitudinal data.

E.3 How does the number of inducing points M affects the overall performance of L-DKGPR?

The number of inducing points provides a trade-off between approximation accuracy and efficiency in sparse GP methods. In this experiment, we vary the number of inducing points from 5 – 100 on simulated data and record the R^2 as shown in Figure 4. We find that when the number of inducing points is above a certain threshold, *i.e.*, 10 in *all* simulated settings, the regression performance is rather stable regardless the increasing of inducing points. A theoretical study [?] points out that when input data are normally distributed and inducing points are drawn from a k -deterministic point process (k -DPP) over K_{XX} with an SE-ARD kernel, then as $N \rightarrow \infty$, $M = \mathcal{O}(\log^P N)$ where P is the input dimension. In our case, if we treat the latent representation as the input dimension as considered in [?], then the number of inducing points suffice to our simulated data should be $M = \log^{10}(1600)$, which is unacceptably large. In contrast, we empirically show that $M \approx \log N$ is sufficient to get appealing results. We conjecture that this is because instead of drawing the inducing points from a k -DPP process from the input data, we optimize representation of the inducing points jointly with the other model parameters, thus delivering more effective inducing points that summarize the variance of the input data.

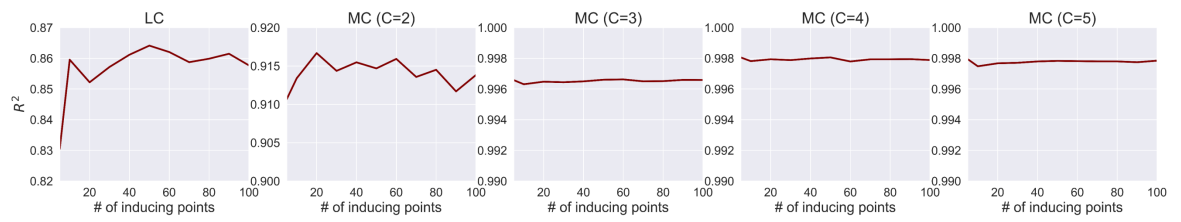


Figure 4: Regression performance with different numbers of inducing points on simulated data.